Physics of the Earth and Planetary Interiors 282 (2018) 39–48

Contents lists available at ScienceDirect

Physics of the Earth and Planetary Interiors

journal homepage: www.elsevier.com/locate/pepi

Temporal change of upper-crustal V_P/V_S ratios with volcanic evolution in Redoubt Volcano

Seongjun Park[a], Tae-Kyung Hong[a,*], Helena Buurman[b]

[a] Yonsei University, Department of Earth System Sciences, 50 Yonsei-ro, Seodaemun-gu Seoul 120-749, South Korea
[b] Alaska Earthquake Center, Geophysical Institute, University of Alaska Fairbanks, 903 Koyukuk Drive, Fairbanks, AK 99775-7320, USA

ARTICLE INFO

Keywords:
Redoubt
Volcano
Eruption
V_P/V_S ratio
Monitoring
Seismic properties
Temporal change

ABSTRACT

Volcanic activities accompany changes in the physical and chemical properties of the medium. The ratio between *P*- and *S*-wave velocities, V_P/V_S, is sensitive to the medium property changes. We investigate temporal variations of the V_P/V_S ratios in the upper crust around Redoubt Volcano in the 1989–2014 time period using the traveltimes of local earthquakes. The V_P/V_S ratios reached ~ 2.0 immediately prior to the 1989–1990 and 2009 eruptions. These high V_P/V_S ratios may be associated with partial melts in the edifice. The V_P/V_S ratios rapidly decreased to ~ 1.7 during the 1989–1990 and 2009 eruptions due to decreasing temperatures, fluids, and pore pressures and increasing effective stresses after melt eruptions and gas emission. The change rates of the V_P/V_S ratios showed evident spatial distributions. The V_P/V_S ratios increased at a rate of 0.025 (±0.003) yr^{-1} below the 2009 vent during the inter-eruption period between the 1989–1990 and 2009 eruptions due to an increase in the temperature, which may be associated with the recharge of the magma in the lower crust. The increase rate of the V_P/V_S ratios was as low as 0.005 (±0.001) yr^{-1} in the regions located away from the eruption site. The V_P/V_S ratios appear to have increased consistently at a rate of 0.017 (±0.004) yr^{-1} since the 2009 eruption.

1. Introduction

Active volcanoes are monitored year-round to mitigate volcanic hazards. The identification of a volcano is crucial for timely preparation. Most active volcanoes can be characterized by eruptive cycles in which prolonged months- to decades-long periods of quiescence are interspersed with episodes of eruptive activity. Many phenomena, such as ground uplift, gas emission and earthquake activity, can provide insights into the state of a volcano in its eruptive cycle (Young et al., 1998; Chouet et al., 1994; Sparks, 2003; Stephens and Chouet, 2001; Power et al., 2013). Understanding and identifying these characteristics is critical for mitigating volcanic hazards.

Eruptive cycles can be characterized by the significant changes in medium properties, including the chemical composition, temperature, local stress field, porosity, density, cracks, and fluid saturation (Wiemer and McNutt, 1997; Rubin et al., 1998; Roman et al., 2004; Sánchez et al., 2004; Pieri and Abrams, 2005; Koulakov et al., 2013; Hong et al., 2014). Seismic properties are sensitive to the properties of the medium (Brenguier et al., 2008; Duputel et al., 2009). The ratio between *P*- and *S*-wave velocities, the V_P/V_S ratio, is sensitive to the medium composition and fluid content and is therefore useful for monitoring the state of a volcano at any given point in its eruptive cycle (Nakajima and Hasegawa, 2003; Chiarabba and Moretti, 2006; Koulakov et al., 2013; Hong et al., 2014).

Volcanic regions are typically characterized by low seismic velocity zones beneath the volcanoes, which indicate the presence of magma (e.g., Nakajima et al., 2001; Sudo and Kong, 2001; Nakajima and Hasegawa, 2003; Koulakov et al., 2007; Koulakov et al., 2009; Lees, 2007; Prôno et al., 2009). The magmas also exhibit high V_P/V_S ratios (Nakajima et al., 2001; Sudo and Kong, 2001; Nakajima and Hasegawa, 2003; Judenherc and Zollo, 2004; Koulakov et al., 2009; Hong et al., 2014). Calderas are generally composed of sediments with open cracks and present low seismic velocities and V_P/V_S ratios (Nakajima and Hasegawa, 2003; Sherburn et al., 2003; Judenherc and Zollo, 2004; Lees, 2007; Koulakov et al., 2009). Non-molten intrusives feature high seismic velocities and V_P/V_S ratios (Sherburn et al., 2003; Judenherc and Zollo, 2004; Prôno et al., 2009). The seismicity, migration and intrusion of magma, fluid transport, heat transfer, and collapse of calderas perturb the medium properties, producing complex seismic velocity structures in the volcanic regions (Nakajima et al., 2001; Sudo and Kong, 2001; Nakajima and Hasegawa, 2003; Koulakov et al., 2009; Sherburn et al., 2003). Investigations of seismic velocities are useful for deducing the structures in volcanic areas. However, the seismic velocity changes during the eruptive cycle of volcanoes are only partially

* Corresponding author.
E-mail addresses: seongjunpark@yonsei.ac.kr (S. Park), tkhong@yonsei.ac.kr (T.-K. Hong), hmbuurman@alaska.edu (H. Buurman).

https://doi.org/10.1016/j.pepi.2018.07.003
Received 6 March 2018; Received in revised form 5 July 2018; Accepted 5 July 2018
Available online 07 July 2018
0031-9201/

understood.

The earthquake catalog from Redoubt Volcano is ideal for studying the eruptive cycle of a stratovolcano. Because Redoubt Volcano has been seismically monitored since 1989, the data set includes two major eruptions between extended periods of quiescence. Both the 1989–1990 and 2009 eruptions were accompanied by lava dome growth and magmatic explosions. The recent eruptions were monitored by a seismic network, providing the opportunity to investigate the changes in the seismic properties accompanying the volcanic activities (Power et al., 1994). Noticeable changes in the seismic velocities, stress fields, seismicity, event characteristics, and V_P/V_S ratios were reported during the eruptions (Stephens et al., 1994; Benz et al., 1996, Sáchez et al., 2004; Buurman et al., 2013b; Ketner and Power, 2013; Kasatkina et al., 2014). However, the temporal evolution of seismic properties within the volcanic edifice during the inter-eruption periods is poorly understood.

In this study, we investigate the V_P/V_S ratios in Redoubt Volcano recorded between 1989 and 2014. The V_P/V_S ratios are estimated using a modified Wadati analysis based on P and S traveltimes. We examine the correlation between the eruptive cycle and the V_P/V_S ratios. We also compare the changes of the V_P/V_S ratios during and after the eruptions to determine the dependence of the V_P/V_S ratios on the eruptive processes.

2. Geology and eruption history

Redoubt Volcano is an active stratovolcano located ~170 km southwest of Anchorage (Fig. 1). The volcano was formed by multiple eruptions. Most silicic parts of the volcano were formed by a large eruption that occurred 0.888 Ma (Till et al., 1994). The sequence includes the Proterozoic basement rock, mid-Pleistocene to Holocene dacitic and basaltic pyroclastic density current deposits, block and ash deposits, and lava flows formed in Jurassic tonalites. The height of the summit of the volcano is 3108 m, and the diameter of the base at the altitude of 1200–1500 m is 10 km (Schaefer, 2011; Grapenthin et al., 2013). The diameter of the summit crater is 1.5 km, and the summit is covered by ice.

Redoubt Volcano erupted in 1902, 1933, and 1966–1968 and recently in 1989–1990 and 2009. The last two eruptions were well monitored (Power et al., 1994; Power et al., 2013; Stephens and Chouet, 2001; Grapenthin et al., 2013; Bull and Buurman, 2013). In the last two eruptions, gas and andesitic lavas explosively erupted through the same vent in the northwest of the volcano (Bull and Buurman, 2013; Diefenbach et al., 2013). The eruptions produced ash clouds, pyroclastic flows, debris flows, and prolonged episodes of lava dome growth (Page et al., 1994; Woods and Kienle, 1994). Both of the recent eruptive episodes at Redoubt Volcano were accompanied by extensive seismicity, including volcanic tremor, long-period seismic events and volcano-tectonic earthquakes that were likely associated with magma migration (Lahr et al., 1994; Chouet, 1996; Morrissey and Chouet, 1997; Buurman et al., 2013b; Grapenthin et al., 2013; Power et al., 2013; Power et al., 2013;Power et al., 2013).

The eruption periods are divided into precursory periods, explosive periods, and effusive periods (Power et al., 2013; Power et al., 2013). The precursory periods are characterized by increases in seismicity, temperature, gas emission, and ground deformation. High-pressurized gas and magma may erupt during the explosive period. Lava domes grow during the effusive period. Precursory activity, including eruptive processes, volcano-tectonic earthquakes, long-period events, volcanic tremor, snow melting, and increased fumarolic activity, was observed from October 1989 to December 14, 1989 prior to the 1989–1990 eruption (Power et al., 1994; Gardner et al., 1994; Schaefer, 2011; Power et al., 2013).

Twenty-five explosive eruptions occurred between December 15, 1989 and April 21, 1990 (Power et al., 1994). The erupted pyroclastic flows with temperatures of 600–700 K reached a height of 12 km (Woods and Kienle, 1994). Following the explosive eruptions, a lava dome grew and failed 13 times until June 15, 1990, defining the effusive period (Page et al., 1994; Miller, 1994). The largest volume of the lava dome was 30 Mm^3 (Miller, 1994). Approximately 88 Mm^3 of magma erupted with an effusion rate of 5.8 m^3/s. The total dense-rock-equivalent volume of the magma that erupted during the 1989–1990 eruption is ~200 Mm^3 (Gardner et al., 1994). The total dense-rock-equivalent volume of the deposits is ~30–50 Mm^3 (Scott and McGimsey, 1994).

The precursory activity leading to the 2009 eruption began in June of 2008. Increased gas flux, ice melting, ground deformation, volcanic tremors, and volcano-tectonic earthquakes were observed at the volcano over a period of nine months prior to the eruption (Schaefer, 2011; Bleick et al., 2013; Grapenthin et al., 2013; Power et al., 2013; Werner et al., 2013). A weak increase of the surface temperatures was also observed (Wessels et al., 2013). Twenty-eight explosive eruptions occurred between March 15, 2009 and April 4, 2009. The eruption column heights reached as high as 19 km during the 2009 eruption (Schneider and Hoblitt, 2013; Wallace et al., 2013). The effusive period followed the explosive eruptions until June, 2009, producing a lava dome with a volume of 72 m^3 (Diefenbach et al., 2013). Approximately 80 Mm^3 of magma erupted with an effusion rate of 9.5 m^3/s (Diefenbach et al., 2013). The total eruption volume of the materials is

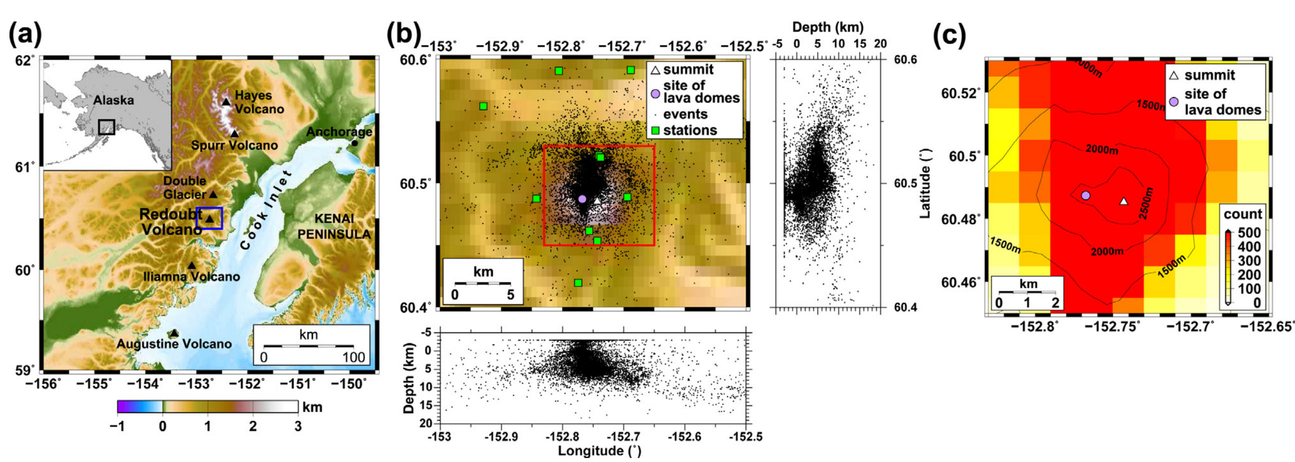

Fig. 1. (a) Map of the major volcanoes in the northeastern Aleutian volcanic arc. A region around Redoubt Volcano is marked with a rectangle. (b) Enlarged map and seismicity around Redoubt Volcano. The locations of the volcano summit (triangle) and the lava domes of the 1989–1990 and 2009 eruptions (circles) are shown. Eleven stations (squares) are available around the volcano. Earthquake depths with latitude and longitude are included as side panels. High seismicity is observed around the volcano. (c) Cell-hit counts of discretized media. The spatial coverage of the raypaths is dense around the summit.

80–120 Mm^3 (Bull and Buurman, 2013). The total dense-rock-equivalent volume of the deposits is ~20.6 Mm^3 (Wallace et al., 2013).

The volcanic eruptions were accompanied by large temporal changes in seismic velocities in the area surrounding Redoubt Volcano. Low seismic velocity anomalies possibly associated with a magma conduit were found at depths of ~1–6 km beneath the volcano during the 1989–1990 eruption (Benz et al., 1996). High seismic velocities and moderate V_P/V_S ratios were observed in the dikes and sills during the inter-eruption period between the 1989–1990 and 2009 eruptions (DeShon et al., 2007). High P velocity anomalies and low S velocity anomalies were observed at the depths of up to ~3 km beneath the summit after the 2009 eruption (Kasatkina et al., 2014). The high V_P/V_S ratios may be caused by magma and fluid-saturated rocks (Kasatkina et al., 2014; Hong et al., 2014).

3. Data

The Alaska Volcano Observatory (AVO) has operated a seismic network to monitor Redoubt Volcano since 1989. The last two eruption events in 1989–1990 and 2009 were well recorded by the seismic network. The seismic stations are well distributed around the volcano. A total of 17013 P and S traveltime pairs were collected from 11 stations between 1989 and 2014 for 7616 local seismic events (Fig. 1). Most earthquake activity occurred during the eruption periods (Fig. 2).

Relatively few events occurred during the inter-eruption period. The focal depths of the events range between −3 and 16.6 km. The magnitudes (M_L) of the events range between −0.9 and 2.4. Most epicentral distances of the data set are less than 10 km. The spatial coverage of the raypaths is dense in the region around the volcano (Fig. 1).

Based on the eruption stages, we divide the data set into 9 subsets. Periods I, II, and III are the precursory, explosive, and effusive periods, respectively, of the 1989 −1990 eruption event (Fig. 2(a)). Periods VI, VII, and III are the precursory, explosive, and effusive periods, respectively, of the 2009 eruption event. Periods IV and V are the inter-eruption periods. Period XI is the post-eruption period following the 2009 eruption.

4. Method and process

We determine the V_P/V_S ratio from the P and S traveltimes of local events using a modified Wadati analysis (Jo and Hong, 2013; Hong et al., 2014):

$$\frac{T_S - T_P}{T_P} = \frac{V_P}{V_S} - 1, \tag{1}$$

where T_P and T_S are the P and S traveltimes. The ratio $\frac{T_S - T_P}{T_P}$ can be determined using linear least-squares fitting and is shown as the slope of the fitted line in the modified Wadati diagram (Fig. 3). A representative V_P/V_S ratio is calculated for each region. To obtain a stable result, we apply an iterative approach for the determination of the V_P/V_S ratio by removing the data points with large traveltime errors (Jo and Hong, 2013; Hong et al., 2014) (Fig. 3).

The V_P/V_S ratio varies strongly with the fluid content in the medium, as observed in volcanic and geothermal regions (Nakajima et al., 2001; Sudo and Kong, 2001; Nakajima and Hasegawa, 2003; Hauksson and Unruh, 2007; Lees, 2007; Koulakov et al., 2009; Raharjo et al., 2016). It was reported that the V_P/V_S ratios are also controlled by the temperature, effective stress, mineral composition, pore pressure, pore density,

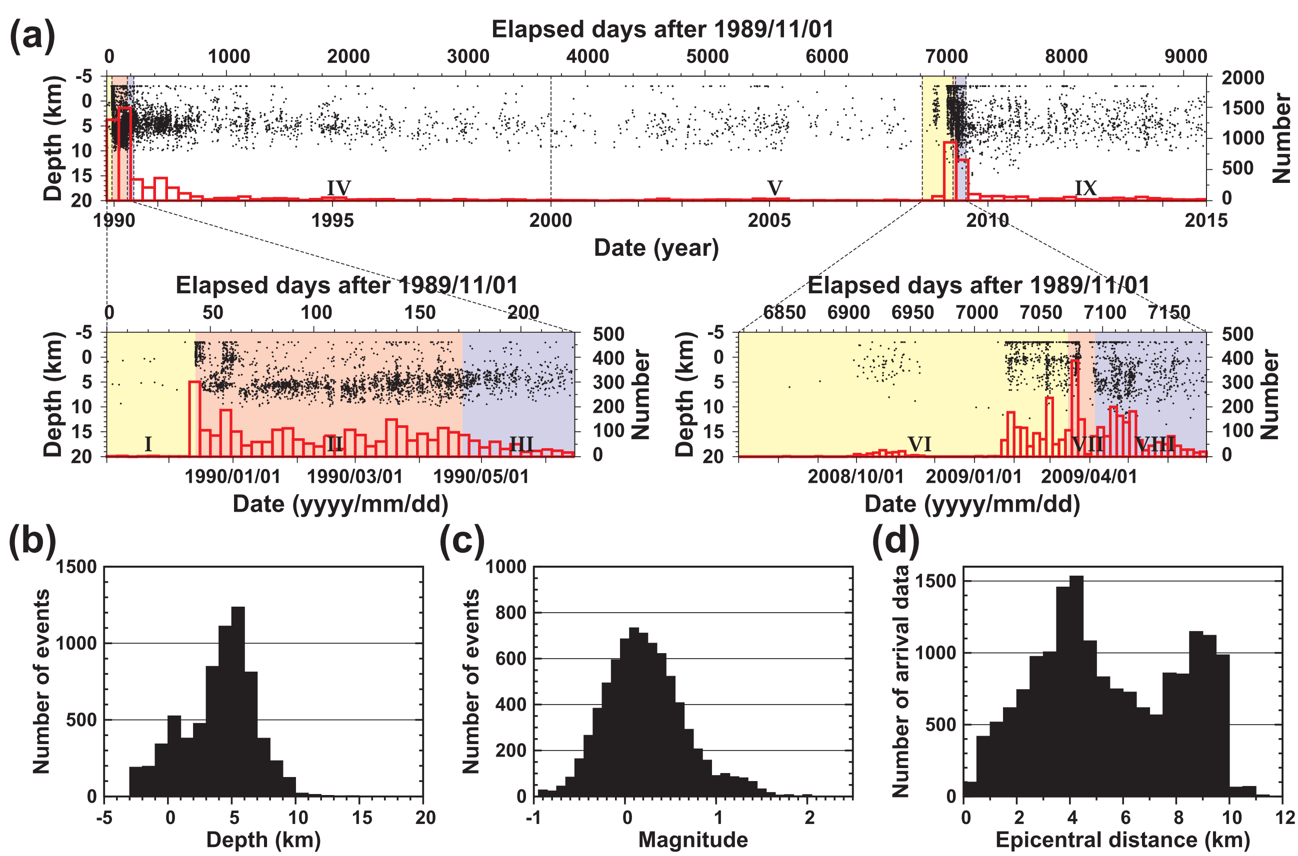

Fig. 2. (a) Distribution of the focal depths of the events used in this study with time during the 1989–2014 time period (top) and the 1989–1990 (bottom left) and 2009 (bottom right) eruptions. The numbers of events in every 100 (top) and 5 (bottom) days are marked with boxes. The precursory, explosive, and effusive periods are indicated (shaded periods). Many earthquakes occur during the eruption periods, while a small number of events are reported for the inter-eruption periods. (b) Focal depth and (c) magnitude distribution of the events. Most focal depths are less than 10 km. The event magnitudes are generally less than 1.5. (d) Distribution of epicentral distances of P- and S-wave traveltime pairs. Most epicentral distances are less than 10 km.

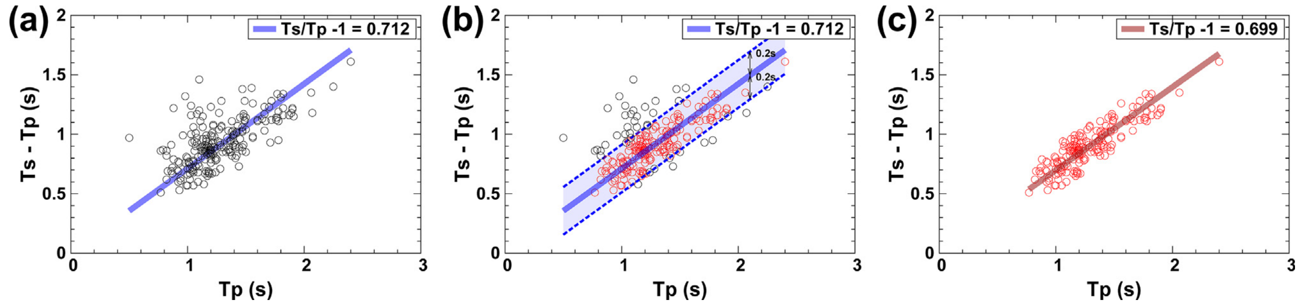

Fig. 3. An example of the V_P/V_S determination procedure using a modified Wadati analysis. (a) Determination of a least-squares fitting line, the slope of which is given by $\frac{V_P}{V_S}-1$. All of the data, including the outliers, contribute to the regression. (b) Exclusion of the outliers with deviations equal to or greater than 0.2 s (marked with dotted lines) from the determined line. (c) Redetermination of the least- squares fit line based on the remaining data. The refinement process is repeated until no further data are excluded.

and crack density (Eberhart-Phillips et al., 1989; Julian et al., 1996; Nakajima et al., 2001; Sudo and Kong, 2001; Takei, 2002; Gunasekera et al., 2003; Nakajima and Hasegawa, 2003; Sherburn et al., 2003; Unglert et al., 2011; Muksin et al., 2013). Temporal changes in the V_P/V_S ratios accompanying temporal changes in the medium properties were widely observed in active volcanoes and geothermal areas (Julian et al., 1996; Gunasekera et al., 2003; Londoño and Makario, 2010; Koulakov et al., 2013).

The V_P/V_S ratios were determined for each period (Fig. 4). The studied region is discretized into spatial bins (cells) with a uniform size of 0.05° in longitude and 0.025° in latitude (Fig. 5), allowing us to investigate the lateral variation of the V_P/V_S ratios. The bins are shifted by 0.02° in longitude and 0.01° in latitude, overlapping with adjacent bins by 0.03° in longitude and 0.015° in latitude.

We select events with focal depths of less than 8 km, naturally constraining the depth of imaging. It is noteworthy that the magma chamber beneath Redoubt Volcano may be located at depths of 3–9 km (Power et al., 2013). The epicentral distances of the data sets are less than 5 km. With the exception of the data subset for period V around the summit, more than 50 data points are present in each subset.

The V_P/V_S ratios are estimated within each data subset throughout the volcanic edifice. The estimated V_P/V_S ratios are refined iteratively based on a modified Wadati analysis by excluding the data points for which the deviation from the initially determined reference line is greater than 0.2 s (Fig. 3). We repeat the refinement procedure until no further data are excluded in the analysis (Hong et al., 2014). With the

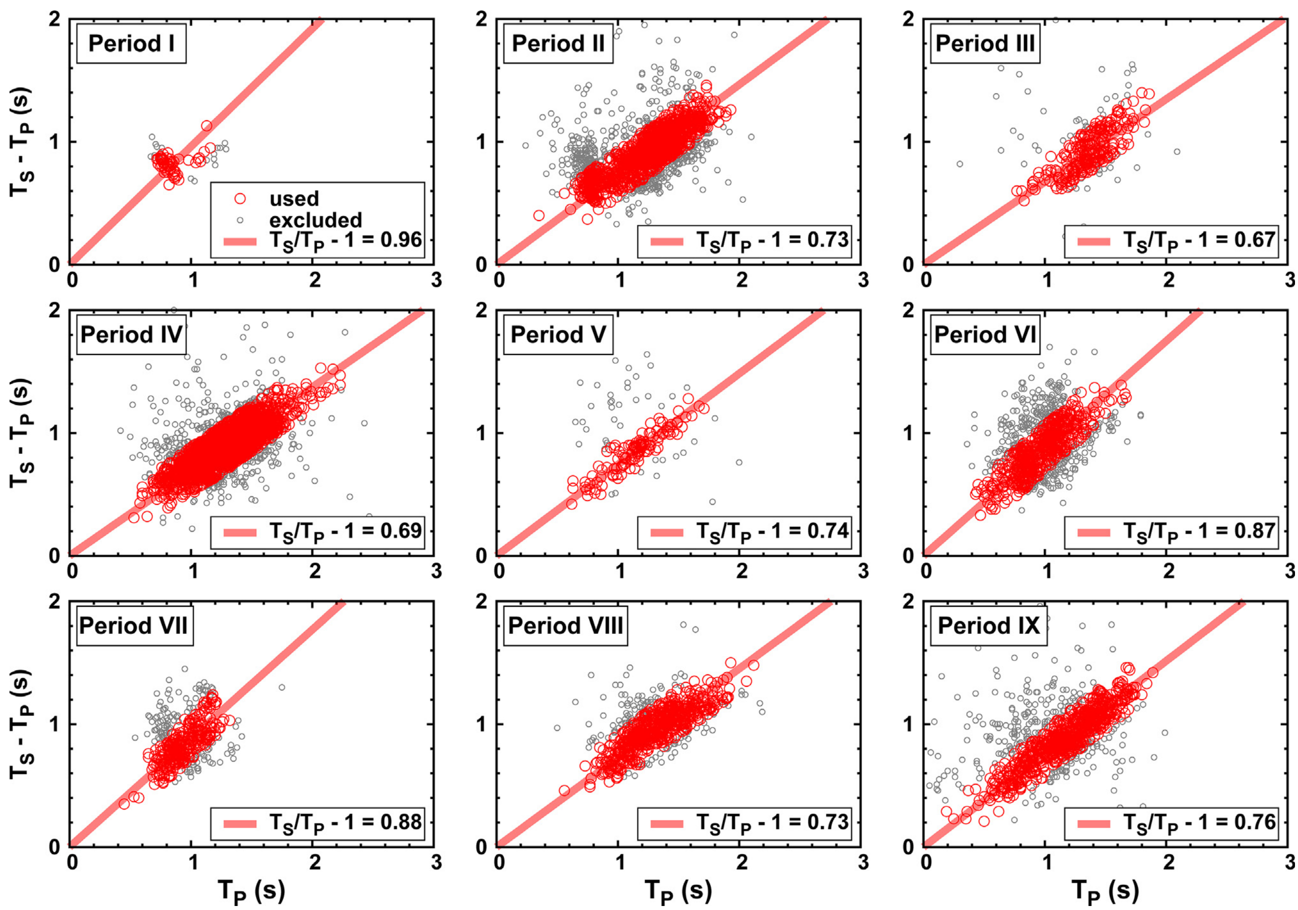

Fig. 4. Determination of the average upper-crustal V_P/V_S ratios for periods I-IX. The slopes of the lines correspond to $\frac{V_P}{V_S}-1$. The outlier data points (small circles) are excluded in the analysis.

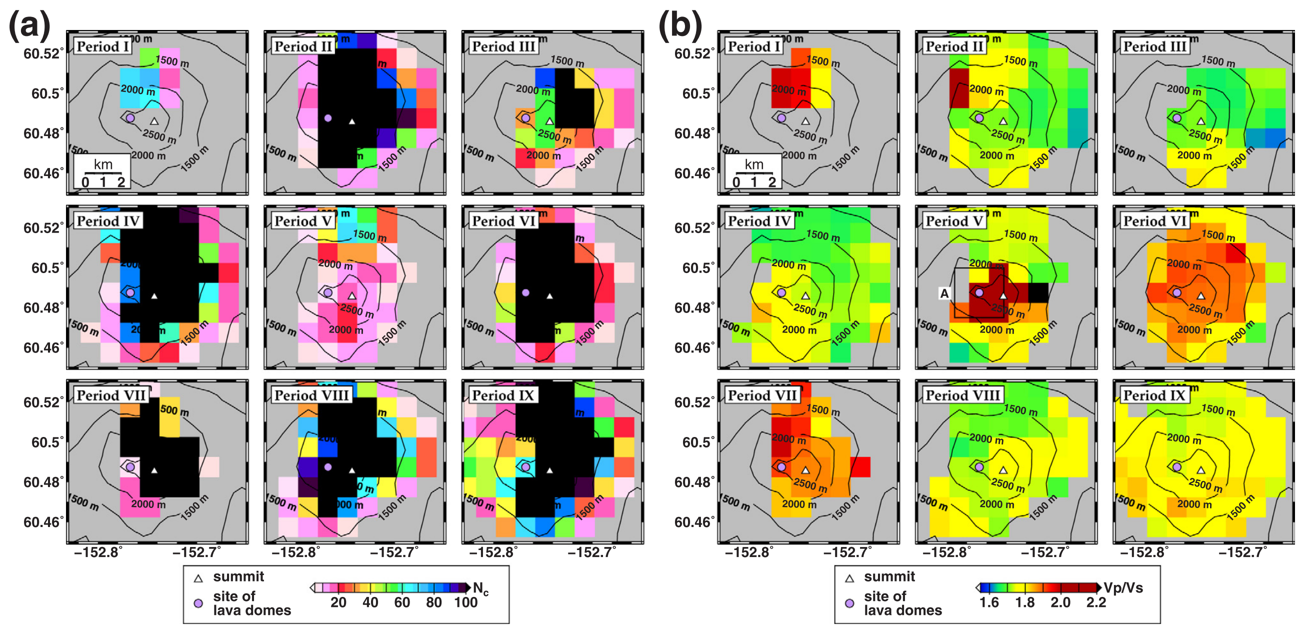

Fig. 5. (a) Number of traveltime pairs (N_c) used for the calculation of the V_P/V_S ratios. The surface topography is marked with contours. Many data points are observed around the summit in all periods except period V. (b) Spatial variations in the V_P/V_S ratios for each time period. The vent (region A) is marked with a box. The V_P/V_S ratios vary significantly with the eruption phase of the volcano. The positions of the summit (triangle) and lava domes (circle) are marked.

exception of the data subset for period V, the traveltime data subsets contain more than 100 data points (Fig. 5).

5. V_P/V_S ratios

We observe significant V_P/V_S ratio changes during volcanic activities (Fig. 4). We also observe apparent spatial variations in the V_P/V_S ratios (Fig. 5). The V_P/V_S ratios increase to ~2.1 over period I (the precursory period of the 1989–1990 eruption), accompanying high seismicity (Fig. 2). This observation suggests that high V_P/V_S ratios may be associated with magma development in the shallow crust (Power et al., 2013). The V_P/V_S ratios for period II (the explosive period of the 1989–1990 eruption) range between 1.7 and 1.8, lower than those for period I. The relatively low V_P/V_S ratios may be associated with the gas emission and magma eruption that result in a decrease in the pore pressure and in the amount of the fluid within the medium (Hong et al., 2014).

The V_P/V_S ratios for period III (the effusive period of the 1989–1990 eruption) are 1.7–1.8, similar to those for period II. The V_P/V_S ratios for period IV (the first half of the inter-eruption period between the 1989–1990 and 2009 eruptions) are 1.7–1.9, and those for period V (the second half of the inter-eruption period) are 1.8–2.2. High V_P/V_S ratios are observed around the 1989–1990 and 2009 eruption vents (region A on the map in Fig. 5(b)). These observations suggests that the V_P/V_S ratios increased during the inter-eruption period.

The V_P/V_S ratios for periods VI and VII (precursory and explosive periods of the 2009 eruption) are 1.9–2.1, suggesting a rapid development of the magma in the shallow crust (Diefenbach et al., 2013; Power et al., 2013). The observed high V_P/V_S ratios during the eruptions are consistent with the results of previous studies (Koulakov et al., 2013; Hong et al., 2014; Kasatkina et al., 2014). The V_P/V_S ratios for period VIII (effusive period of the 2009 eruption) are 1.7–1.8. The decreasing V_P/V_S ratios may suggest a reduction in the gas and melts in the edifice. Period IX (the post-eruption period after the 2009 eruption) presents V_P/V_S ratios of 1.8–1.9, which are higher than those for period VIII, suggesting an increase in the V_P/V_S ratios during the post-eruption period.

6. Stability tests

We verify the results by examining their stability using bootstrap analysis (Efron and Tibshirani, 1991; Jo and Hong, 2013; Hong et al., 2014). Bootstrap analysis generates data sets that are randomly resampled from the original data set while allowing duplicate selection of any data points. The resampled data sets are analyzed, yielding stochastic results. The standard errors among the results based on resampled data sets are assessed, allowing us to examine the stability of the results.

We produce 100 bootstrap data sets for each spatial and temporal window. The mean values of the V_P/V_S ratios obtained using the bootstrap data sets are close to the results obtained using the original data set (Fig. 6). The standard deviations among the bootstrap results are less than 0.05 for most regions and periods except for the results for period V, for which only a small number of data points are available (Fig. 6). The bootstrap test suggests that the results are stable and rarely depend on certain data points.

The V_P/V_S estimates suffer from the errors in the traveltime data associated with phase picking and origin time errors. The influence of the errors on the analysis is examined. The errors in P and S phase picking may be less than 0.05 and 0.1 s, respectively, considering the epicentral distances, focal depths, and sampling rates of the waveforms (Hong et al., 2014). We produce 100 traveltime data sets by adding white noise random errors in the range from −0.05 to 0.05 s for P and from −0.1 to 0.1 s for S traveltimes.

The average differences between the V_P/V_S estimates based on the original data set and those based on the random-error-added data sets are generally less than 0.03 (Fig. 7). The standard deviations of the V_P/V_S estimates among the 100 random-error-added data sets are less than 0.04 for most regions and periods, corresponding to deviations of up to 0.08 in the 95 % confidence interval. This test suggests that the influence of the possible errors in the traveltimes on the results may not be significant.

Errors in the origin times may be associated with event location errors. We examine the influence of origin time errors on the V_P/V_S estimates. We prepare 100 traveltime data sets by adding white noise random errors ranging from −0.2 to 0.2 s to the origin times,

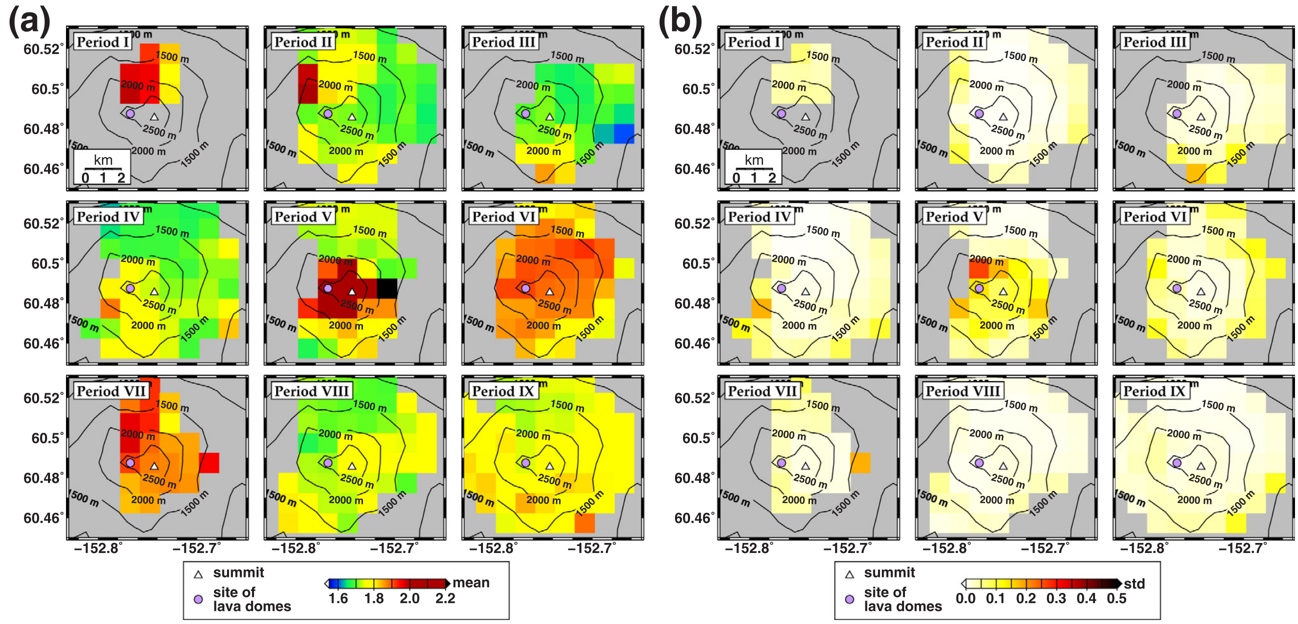

Fig. 6. Bootstrap test of the obtained V_P/V_S ratios. (a) Average of the results from 100 bootstrap data sets. The average values are close to the results from the original data set. (b) Standard deviations among the results obtained from the 100 bootstrap data sets. With the exception of period V, the standard deviations are low in most regions and time periods. The positions of the summit (triangle) and lava domes (circle) are marked.

corresponding to hypocenter errors of up to ~1.5 km in a typical continental crust (Hong et al., 2014). The V_P/V_S ratios are estimated for the error-added data sets (Fig. 8). With the exception of period V, the average differences between the V_P/V_S estimates based on the original data set and those based on the error-added data sets are less than 0.04 for all regions and periods. The standard deviations are also less than 0.06.

We also examine the composite effect of the phase picking and origin time errors on the analysis. We produce 100 traveltime data sets with random errors in the P and S traveltimes and the origin times. The random errors range from −0.05 to 0.05 s for the P traveltimes, from −0.1 to 0.1 s for the S traveltimes, and from −0.2 to 0.2 s for the origin times. We find that the average differences between the V_P/V_S estimates based on the original data set and those based on the random-error-added data sets are less than 0.04 for most regions and periods (Fig. 9). The standard deviations are less than 0.07. This test suggests that the composite effect of the errors in the phase picking and origin times on the results is likely not significant.

7. Temporal variation in V_P/V_S ratios

The V_P/V_S ratios are estimated using every 20 traveltime data points (Fig. 10). Significant temporal variations in the V_P/V_S ratios are observed during the inter-eruption and eruption periods. The reliability of

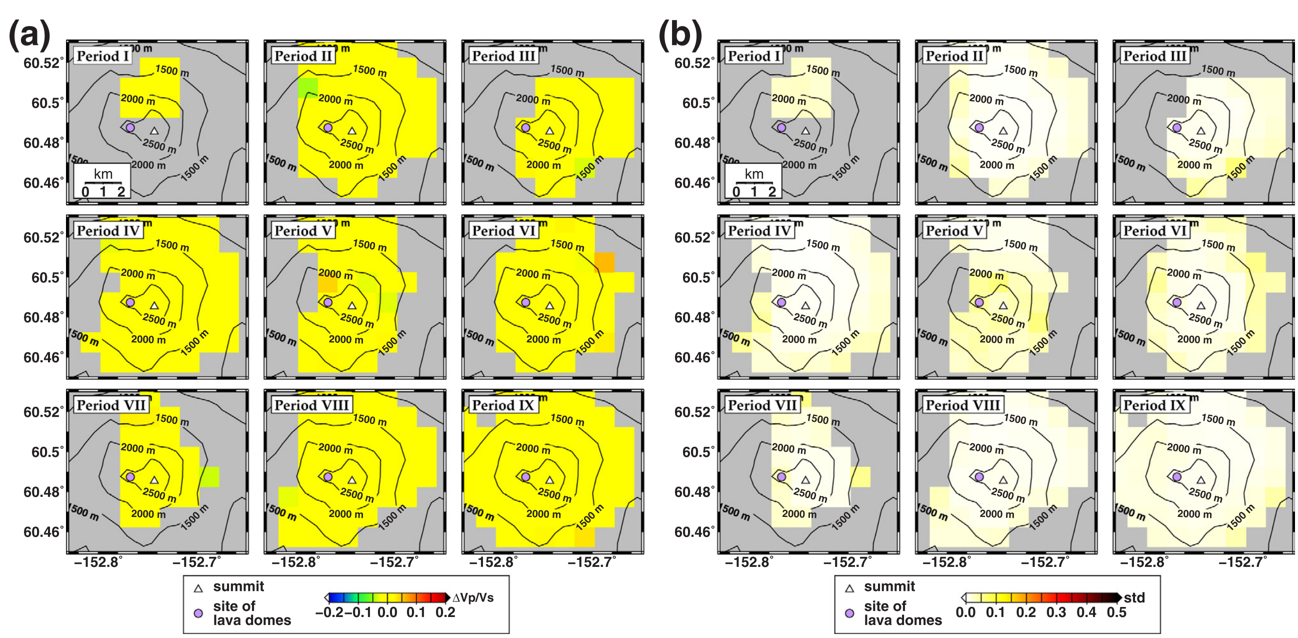

Fig. 7. Examination of the potential influence of phase picking errors on the estimation of the V_P/V_S ratios. (a) Average values and (b) standard deviations of the differences between the results from 100 error-added and original data sets. The average differences are close to zero for most regions and periods. The standard deviations are low in most regions and periods. The positions of the summit (triangle) and lava domes (circle) are marked.

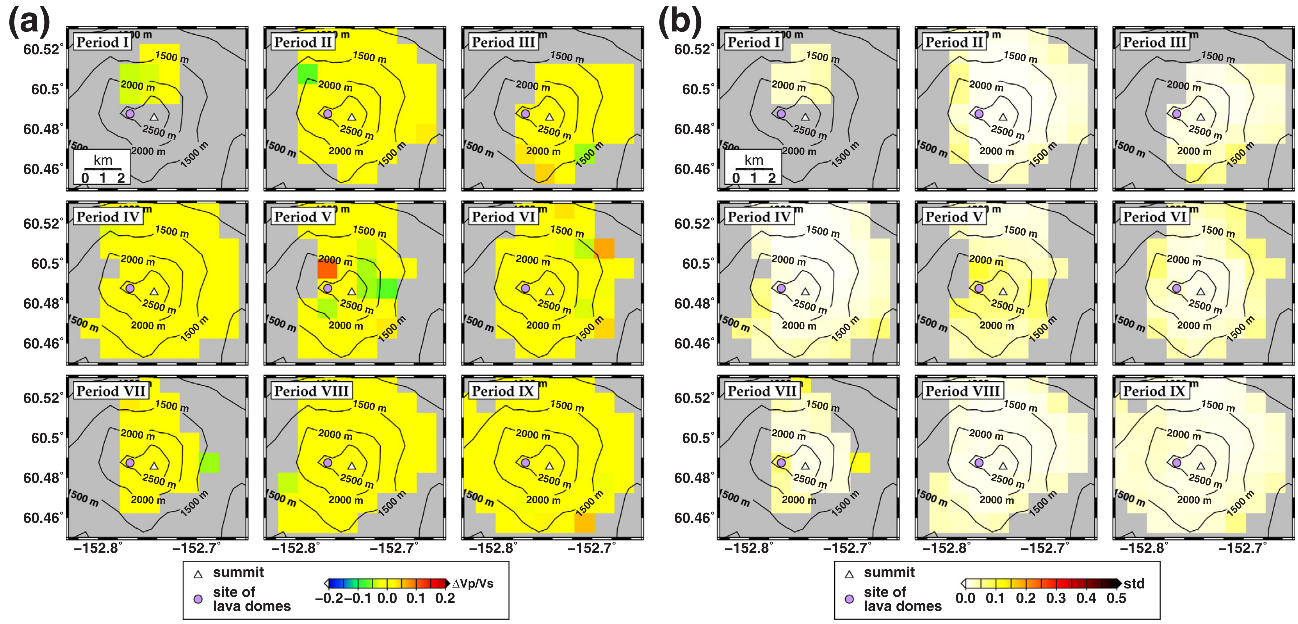

Fig. 8. Examination of the potential influence of origin time errors on the estimation of the V_P/V_S ratios. (a) Average values and (b) standard deviations of the differences between the results from 100 error-added and original data sets. The average differences are close to zero for most regions and periods. The standard deviations are low in most regions and periods. The positions of the summit (triangle) and lava domes (circle) are marked.

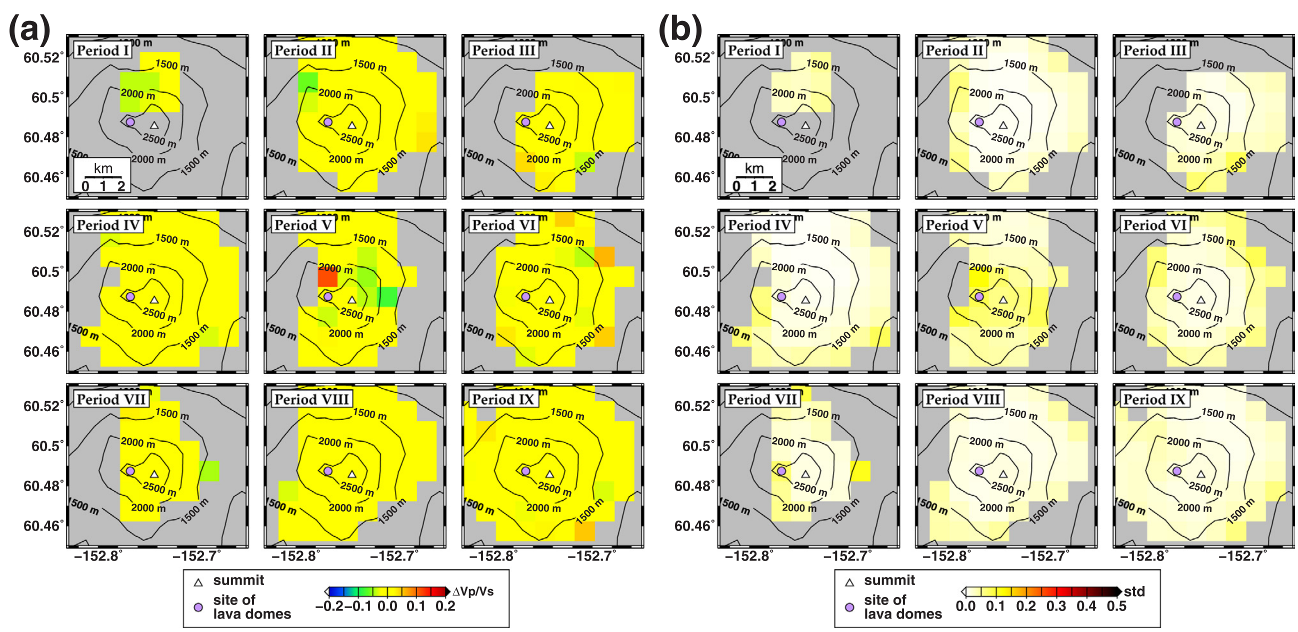

Fig. 9. Examination of the potential composite influence of phase picking and origin time errors on the estimation of the V_P/V_S ratios. (a) Average values and (b) standard deviations of the differences between the results from 100 error-added and original data sets. The average differences are close to zero for most regions and periods. The standard deviations are low in most regions and periods. The positions of the summit (triangle) and lava domes (circle) are marked.

the results is verified using bootstrap analysis (Fig. 11). We produce 100 bootstrap data sets from the original data sets. The average values of the V_P/V_S ratios obtained from the bootstrap data sets agree with the results obtained from the original data sets. The standard deviations are low for most periods except for period V, for which only a small number of data points are available. The test results support the stability of the obtained V_P/V_S ratios.

The V_P/V_S ratios decrease to ~1.7 during the eruptions (periods II-III and VI-VIII), which is consistent with a previous study (Fig. 10) (Hong et al., 2014). The decrease in the V_P/V_S ratios during the precursory period of the 2009 eruption event (period VI) may be associated with the decrease of the pore pressures in the medium due to the emission of overpressurized gas (Power et al., 2013; Hong et al., 2014). However, a decrease in the V_P/V_S ratios is not observed in the precursory period of the 1989–1990 eruption event (period I) due to a different eruption mechanism. It has been suggested that the 1989–1990 eruption was caused by magma mixing (Wolf and Eichelberger, 1997). On the other hand, the 2009 eruption was caused by the remobilization of the residing materials due to the migration of magma from the lower crust (Coombs et al., 2013; Grapenthin et al., 2013; Power et al., 2013).

High V_P/V_S ratios up to ~2.0 were observed prior to the eruptions. A V_P/V_S ratio of 2.0 may suggest a medium porosity of ~ 0.11 when isotropically-distributed pores are filled with melts with a bulk modulus of 10 GPa in a medium with a temperature of 255 °C and a pressure of

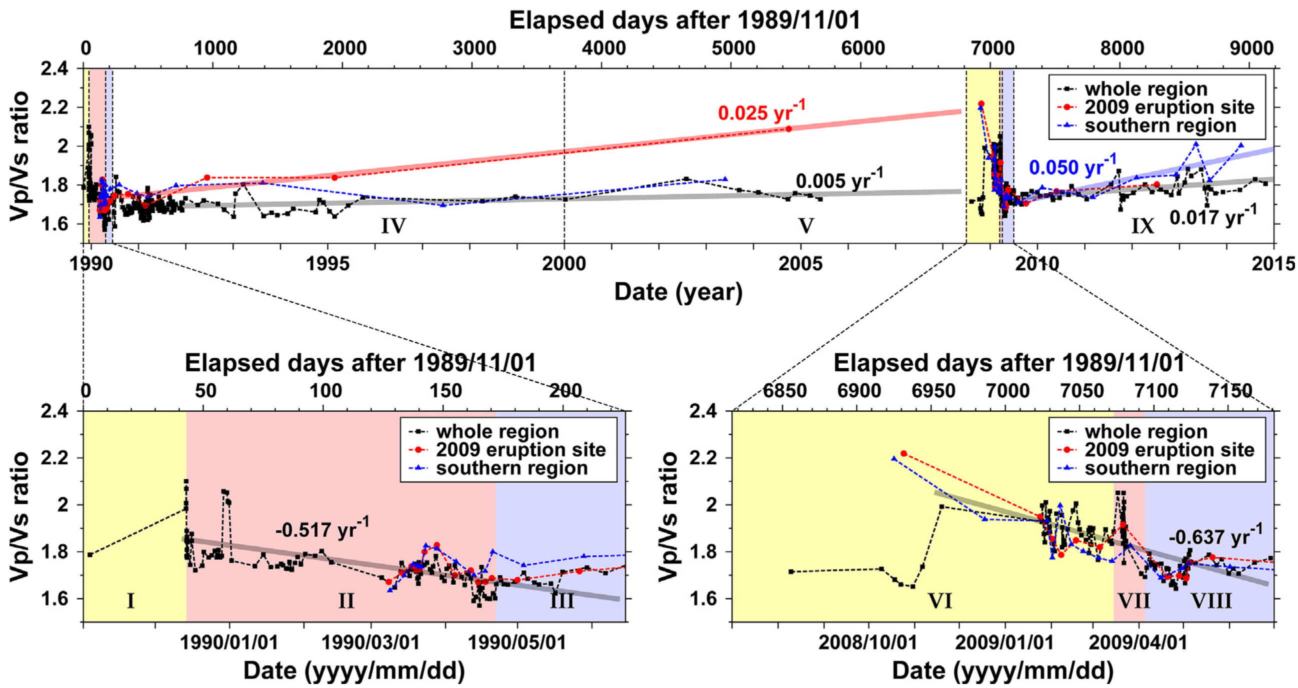

Fig. 10. Temporal variations of the V_P/V_S ratios in the 1990–2015 time period (top). The V_P/V_S ratios during the 1989–1990 (bottom left) and 2009 (bottom right) eruptions are enlarged. The average V_P/V_S ratios for the whole region (squares), the region of the 2009 eruption (region A, circles) and the southern region of the volcano (region B, triangles) are shown. The precursory, explosive, and effusive periods are indicated. The least-squares fitting lines (solid lines) and their slopes for the inter-eruption periods and eruption periods are shown. The V_P/V_S ratios decrease during the eruptions and increase during the inter-eruption periods.

0.13 GPa (Gassmann, 1951; Husen et al., 2004; Hong et al., 2014).

The V_P/V_S ratios decreased rapidly during the explosive and effusive periods. The decreasing V_P/V_S ratios may be attributed to decreases in the amounts of the partial melts in the edifice (Christensen, 1996; Chiarabba and Moretti, 2006; Hong et al., 2014; Kasatkina et al., 2014). The eruption volumes were 200 and 80–120 Mm^3 (Gardner et al., 1994; Bull and Buurman, 2013). The magma discharge also decreases the tensional strain and temperature in the medium, consequently reducing the V_P/V_S ratios (Mogi, 1958; Eberhart-Phillips et al., 1989; Reid, 2004; Sánchez et al., 2004). The compressional stress may have increased by ~5 MPa during the 2009 eruption (Sánchez et al., 2004).

The V_P/V_S ratios increase during the inter-eruption periods (Fig. 10). The V_P/V_S ratios generally increase during periods IV-V at a rate of 0.005 (±0.001) yr^{-1}, which, however, varies significantly by local region (Fig. 12). We observe a high rate of 0.025 (±0.003) yr^{-1} around the site of the 2009 eruption event (region A). The increase in the V_P/V_S ratios during the inter-eruption period may be associated with the increase of the temperature in the volcanic edifice, which may in turn may be associated with the recharge of magma in the magma chamber in the deep crust. It was proposed that magma ascended from the deep crust to the shallow magma chamber at the depth of 3–6 km prior to the 2009 eruption (Coombs et al., 2013; Grapenthin et al., 2013).

We find that the V_P/V_S ratios increased in the post-eruption period after the 2009 eruption event (Fig. 12). The average increase rate over the whole region is 0.017 (±0.004) yr^{-1}. A high increase rate of 0.050 (±0.015) yr^{-1} is observed in the southern region of the volcano (region B) (Fig. 12). The increase in the V_P/V_S ratios is likely associated with the temperature changes beneath the volcano. A high surface temperature was observed around the volcano after the 2009 eruption (Wessels et al., 2013). This observation may be associated with the magma movement beneath the volcano after the 2009 eruption (Buurman et al., 2013a). The difference in the increase rates after the two eruptions may

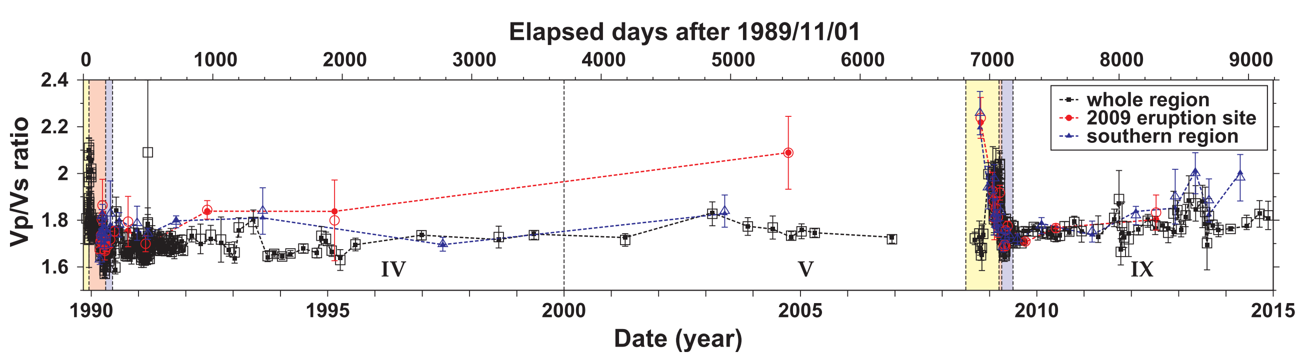

Fig. 11. Bootstrap test of the temporal variations in the V_P/V_S ratios. The average values of the results obtained from 100 bootstrap data sets are presented with standard deviations (bars): the entire region (open squares), the region of the 2009 eruption (region A, circles), and the southern region of the volcano (region B, triangles). The results from the original data sets are represented by closed symbols. The average values of the results obtained from the bootstrap data sets are close to the results obtained from the original data sets. The standard deviations are low in most periods

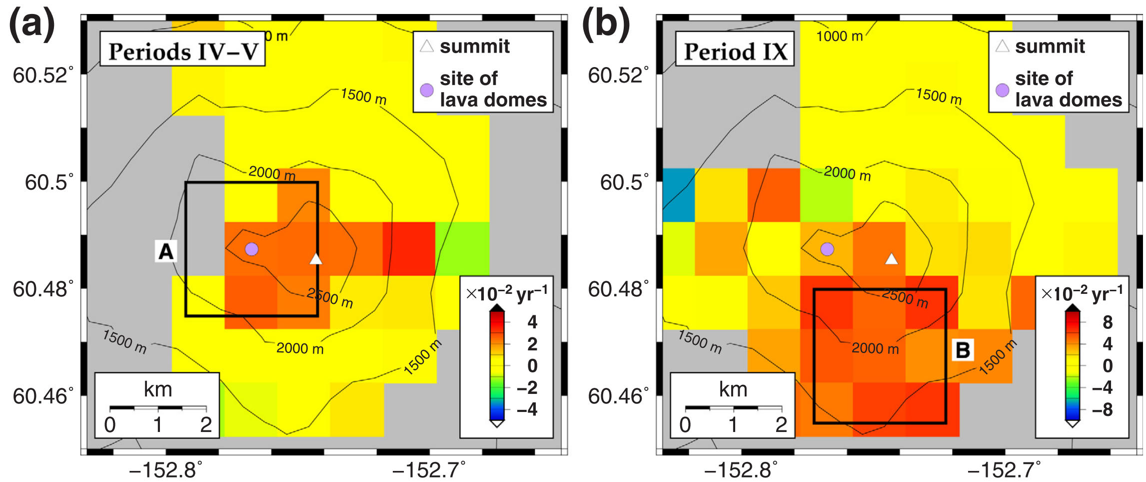

Fig. 12. Spatial variations of the increase rates of the V_P/V_S ratios during (a) periods IV-V and (b) period IX. The increase rates of the V_P/V_S ratios during periods IV-V are high around the region of the 2009 eruption (region A). High increase rates of the V_P/V_S ratios are observed during period IX in the southern region of the volcano (region B). The positions of the summit (triangle) and lava domes (circle) are marked.

be associated with the differences in the recharge rates and the depths of the magma chambers.

8. Discussion and conclusions

We investigated the temporal variation in the V_P/V_S ratios around Redoubt Volcano during the 1989–2014 time period, which includes the 1989–1990 and 2009 eruptions. The V_P/V_S ratios were estimated using a modified Wadati analysis based on the *P* and *S* traveltimes of local earthquakes. The reliability of the results was tested using bootstrap analysis.

We observed temporal changes in the V_P/V_S ratios around the volcano with the eruptive cycle of the volcano. The changes in the medium properties accompanying the volcanic activities control the V_P/V_S ratios. The V_P/V_S ratios increased during the inter-eruption periods and decreased during the eruption periods. The regions with the high increase rates of the V_P/V_S ratios during the inter-eruption period are observed to be associated with the magma development and following eruption. The southern region of the volcano presents a high increase rate of the V_P/V_S ratio during the latest period.

The temperature of the magma was 890–960 °C during the pre-eruption period (Coombs et al., 2013) and then decreased with time. The temperature decrease caused a decrease in the Poisson's ratios (Christensen, 1996; Julian et al., 1996; Sudo and Kong, 2001). The development of cracks may also have contributed to the decrease in the V_P/V_S ratios (Hauksson and Unruh, 2007; Fortin et al., 2007; Unglert et al., 2011; Hong et al., 2014). The decreasing pore pressure and increasing effective stress may have contributed to the decrease in the V_P/V_S ratio (Eberhart-Phillips et al., 1989; Julian et al., 1996; Gunasekera et al., 2003). The increase of the V_P/V_S ratios during the inter- eruption period (periods IV and V) may suggest recharging of the magma. The V_P/V_S ratios may be useful for identification of potential locations of future eruptions.

Acknowledgements

The authors are grateful to Professor Vernon Cormier (editor) and an anonymous reviewer for valuable review comments that improved the presentation of this manuscript. This work was supported by the Korea Meteorological Administration Research and Development Program under Grant KMI2018-02910. In addition, this research was partly supported by the Basic Science Research Program through the National Research Foundation of Korea (NRF) funded by the Ministry of Education (NRF-2017R1A6A1A07015374).

Appendix A. Supplementary data

Supplementary data associated with this article can be found, in the online version, athttps://doi.org/10.1016/j.pepi.2018.07.003.

References

Benz, H.M., Chouet, B.A., Dawson, P.B., Lahr, J.C., Page, R.A., J.A., 1996. Three-dimensional P and S wave velocity structure of Redoubt Volcano, Alaska. J. Geophys. Res. 101, 8111–8128.
Brenguier, F., Shapiro, N.M., Campillo, M., Ferrazzini, V., Duputel, Z., Coutant, O., Nercessian, A., 2008. Towards forecasting volcanic eruptions using seismic noise. Nat. Geosci. 1, 126–130.
Bleick, H.A., Coombs, M.L., Cervelli, P.F., Bull, K.F., Wessels, R.L., 2013. Volcano-ice interactions precursory to the 2009 eruption of Redoubt Volcano, Alaska. J. Volcanol. Geotherm. Res. 259, 373–388.
Bull, K.F., Buurman, H., 2013. An overview of the 2009 eruption of Redoubt Volcano, Alaska. J. Volcanol. Geotherm. Res. 259, 2–15.
Buurman, H., West, M.E., Roman, D.C., 2013a. Using repeating volcano-tectonic earthquakes to track post-eruptive activity in the conduit system at Redoubt Volcano, Alaska. Geology 41, 511–514.
Buurman, H., West, M.E., Thompson, G., 2013b. The seismicity of the 2009 Redoubt eruption. J. Volcanol. Geotherm. Res. 259, 16–30.
Chiarabba, C., Moretti, M., 2006. An insight into the unrest phenomena at the Campi Flegrei caldera from V_P and V_P/V_S tomography. Terra Nova 18, 373–379.
Chouet, B.A., 1996. Long-period volcano seismicity: its source and use in eruption forecasting. Nature 380, 309–316.
Chouet, B.A., Page, R.A., Stephens, C.D., Lahr, J.C., Power, J.A., 1994. Precursory swarms of long-period events at Redoubt Volcano (1989–1990), Alaska: Their origin and use as a forecasting tool. J. Volcanol. Geotherm. Res. 62, 95–135.
Christensen, N.I., 1996. Poisson's ratio and crustal seismology. J. Geophys. Res. 10, 3139–3156.
Coombs, M.L., Sisson, T.W., Bleick, H.A., Henton, S.M., Nye, C.J., Payne, A.L., Camerond, C.E., Larsenc, J.F., Wallacea, K.L., Bull, K.F., 2013. Andesites of the 2009 eruption of Redoubt Volcano, Alaska. J. Geophys. Res. 259, 349–372.
DeShon, H.R., Thurber, C.H., Rowe, C., 2007. High-precision earthquake location and three-dimensional P wave velocity determination at Redoubt Volcano, Alaska. J. Geophys. Res. 112, B07312. https://doi.org/10.1029/2006JB004751.
Diefenbach, A.K., Bull, K.F., Wessels, R.L., McGimsey, R.G., 2013. Photogrammetric monitoring of lava dome growth during the 2009 eruption of Redoubt Volcano. J. Volcanol. Geotherm. Res.. 259, 308–316.
Duputel, Z., Ferrazzini, V., Brenguier, F., Shapiro, N., Campillo, M., Nercessian, A., 2009. Real time monitoring of relative velocity changes using ambient seismic noise at the Piton de la Fournaise volcano (La Réunion) from January 2006 to June 2007. J. Volcanol. Geotherm. Res.. 184, 164–173.
Eberhart-Phillips, D., Han, D.H., Zoback, M.D., 1989. Empirical relationships among seismic velocity, effective pressure, porosity, and clay content in sandstone. Geophysics 54, 82–89.
Efron, B., Tibshirani, R., 1991. Statistical data analysis in the computer age. Science 253, 390–395.
Fortin, J., Guéguen, Y., Schubnel, A., 2007. Effects of pore collapse and grain crushing on ultrasonic velocities and V_P/V_S. J. Geophys. Res. 112, B08207. https://doi.org/10.1029/2005JB004005.
Gardner, C.A., Neal, C.A., Waitt, R.B., Janda, R.J., 1994. Proximal pyroclastic deposits from the 1989–1990 eruption of Redoubt Volcano, Alaska- stratigraphy, distribution,

and physical characteristics. J. Volcanol. Geotherm. Res. 62, 213–250.
Gassmann, F., 1951. Uber die Elastizitat proser Medien. Viertel. Naturforsch. Ges. Zürich. 96, 1–23.
Grapenthin, R., Freymueller, J.T., Kaufman, A.M., 2013. Geodetic observations during the 2009 eruption of Redoubt Volcano, Alaska. J. Volcanol. Geotherm. Res. 259, 115–132.
Gunasekera, R.C., Foulger, G.R., Julian, B.R., 2003. Reservoir depletion at The Geysers geothermal area, California, shown by four-dimensional seismic tomography. J. Geophys. Res.: Solid Earth 108, 2134. https://doi.org/10.1029/2001JB000638.
Hauksson, E., Unruh, J., 2007. Regional tectonics of the Coso geothermal area along the intracontinental plate boundary in central eastern California: Three-dimensional V_P and V_P/V_S models, spatial-temporal seismicity patterns, and seismogenic deformation. J. Geophys. Res.: Solid Earth 112, B06309. https://doi.org/10.1029/2006JB004721.
Husen, S., Smith, R.B., Waite, G.P., 2004. Evidence for gas and magmatic sources beneath the Yellowstone volcanic field from seismic tomographic imaging. J. Volcanol. Geotherm. Res. 131, 397–410.
Hong, T.-K., Houng, S.E., Jo, E., 2014. Temporal changes of medium properties during explosive volcanic eruption. Geophys. Res. Lett. 41, 1944–1950. https://doi.org/10.1002/2014GL059408.
Jo, E., Hong, T.-K., 2013. V_P/V_S ratios in the upper crust of the southern Korean Peninsula and their correlations with seismic and geophysical properties. J. Asian Earth Sci. 66, 204–214.
Judenherc, S., Zollo, A., 2004. The Bay of Naples (southern Italy): constraints on the volcanic structures inferred from a dense seismic survey. J. Geophys. Res.: Solid Earth 109, B10312. https://doi.org/10.1029/2003JB002876.
Julian, B.R., Ross, A., Foulger, G.R., Evans, J.R., 1996. Three-dimensional seismic image of a geothermal reservoir: the Geysers, California. Geophys. Res. Lett. 23, 685–688.
Kasatkina, E., Koulakov, I., West, M., Izbekov, P., 2014. Seismic structure changes beneath Redoubt Volcano during the 2009 eruption inferred from local earthquake tomography. J. Geophys. Res. 119, 4938–4954.
Ketner, D., Power, J., 2013. Characterization of seismic events during the 2009 eruption of Redoubt Volcano, Alaska. J. Volcanol. Geotherm. Res. 259, 45–62.
Koulakov, I., Bohm, M., Asch, G., Lühr, B.G., Manzanares, A., Brotopuspito, K.S., Fauzi, P., Purbawinata., M.A., Puspito, N.T., Ratdomopurbo, A., Kopp, H., Rabbel, W., Shevkunova, E., 2007. P and S velocity structure of the crust and the upper mantle beneath central Java from local tomography inversion. J. Geophys. Res.: Solid Earth 112, B08310. https://doi.org/10.1029/2006JB004712.
Koulakov, I., Gordeev, E.I., Dobretsov, N.L., Vernikovsky, V.A., Senyukov, S., Jakovlev, A., Jaxybulatov, K., 2013. Rapid changes in magma storage beneath the Klyuchevskoy group of volcanoes inferred from time-dependent seismic tomography. J. Volcanol. Geotherm. Res. 263, 75–91.
Koulakov, I., Yudistira, T., Luehr, B.G., 2009. P, S velocity and V_P/V_S ratio beneath the Toba caldera complex (Northern Sumatra) from local earthquake tomography. Geophys. J. Int. 177, 1121–1139.
Lahr, J.C., Chouet, B.A., Stephens, C.D., Power, J.A., Page, R.A., 1994. Earthquake classification, location, and error analysis in a volcanic environment: Implications for the magmatic system of the 1989–1990 eruptions at Redoubt Volcano, Alaska. J. Volcanol. Geotherm. Res. 62, 137–151.
Lees, J.M., 2007. Seismic tomography of magmatic systems. J. Volcanol. Geotherm. Res. 167, 37–56.
Londoño, B., Makario, J., 2010. Activity and V_P/V_S ratio of volcano-tectonic seismic swarm zones at Nevado del Ruiz Volcano, Colombia. Earth Sci. Res. J. 14, 111–124.
Miller, T.P., 1994. Dome growth and destruction during the 1989–1990 eruption of Redoubt Volcano. J. Volcanol. Geotherm. Res. 62, 197–212.
Mogi, K., 1958. Relations between the eruptions of various volcanoes and the deformations of the ground surfaces around them. Bull. Earthq. Res. Inst. 36, 99–134.
Morrissey, M.M., Chouet, B.A., 1997. A numerical investigation of choked flow dynamics and its application to the triggering mechanism of long-period events at Redoubt Volcano, Alaska. J. Geophys. Res. 102, 7965–7983.
Muksin, U., Bauer, K., Haberland, C., 2013. Seismic V_P and V_P/V_S structure of the geothermal area around Tarutung (North Sumatra, Indonesia) derived from local earthquake tomography. J. Volcanol. Geotherm. Res. 260, 27–42.
Nakajima, J., Hasegawa, A., 2003. Tomographic imaging of seismic velocity structure in and around the Onikobe volcanic area, northeastern Japan: implications for fluid distribution. J. Volcanol. Geotherm. Res. 127, 1–18.
Nakajima, J., Matsuzawa, T., Hasegawa, A., Zhao, D., 2001. Three-dimensional structure of V_P, V_S, and V_P/V_S beneath northeastern Japan: Implications for arc magmatism and fluids. J. Geophys. Res. 106, 21843–21857.
Page, R.A., Lahr, J.C., Chouet, B.A., Power, J.A., Stephens, C.D., 1994. Statistical forecasting of repetitious dome failures during the waning eruption of Redoubt Volcano, Alaska, February-April 1990. J. Volcanol. Geotherm. Res. 62, 183–196.
Pieri, D., Abrams, M., 2005. ASTER observations of thermal anomalies preceding the April 2003 eruption of Chikurachki volcano, Kurile Islands, Russia. Remote Sens. Environ. 99, 84–94.
Prôno, E., Battaglia, J., Monteiller, V., Got, J.L., Ferrazzini, V., 2009. P-wave velocity structure of Piton de la Fournaise volcano deduced from seismic data recorded between 1996 and 1999. J. Volcanol. Geotherm. Res. 184, 49–62.
Power, J.A., Lahr, J.C., Page, R.A., Chouet, B.A., Stephens, C.D., Harlow, D.H., Murray, T.L., Davies, J.N., 1994. Seismic evolution of the 1989–1990 eruption sequence of Redoubt Volcano, Alaska. J. Volcanol. Geotherm. Res. 62, 69–94.
Power, J.A., Stihler, S.D., Chouet, B.A., Haney, M.M., Ketner, D.M., 2013. Seismic observations of Redoubt Volcano, Alaska–1989-2010 and a conceptual model of the Redoubt magmatic system. J. Volcanol. Geotherm. Res. 259, 31–44.
Reid, M.E., 2004. Massive collapse of volcano edifices triggered by hydrothermal pressurization. Geology 32, 373–376.
Raharjo, W., Palupi, I.R., Nurdian, S.W., Giamboro, W.S., Soesilo, J., 2016. Poisson's ratio analysis (V_P/V_S) on volcanoes and geothermal potential areas in Central Java using tomography travel time method of grid search relocation hypocenter. J. Phys.: Conf. Ser. 776, 012114. https://doi.org/10.1088/1742-6596/776/1/012114.
Roman, D.C., Moran, S.C., Power, J.A., Cashman, K.V., 2004. Temporal and spatial variation of local stress fields before and after the 1992 eruptions of Crater Peak vent, Mount Spurr volcano, Alaska. Bull. Seismol. Soc. Am. 94, 2366–2379.
Rubin, A.M., Gillardand, D., Got, J.-L., 1998. A reinterpretation of seismicity associated with the January 1983 dike intrusion at Kilauea Volcano, Hawaii. J. Geophys. Res. 103, 10003–10015.
Sánchez, J.J., Wyss, M., McNutt, S.R., 2004. Temporal-spatial variations of stress at Redoubt volcano, Alaska, inferred from inversion of fault plane solutions. J. Volcanol. Geotherm. Res. 130, 1–30.
Schaefer, J., 2011. The 2009 eruption of Redoubt Volcano, Alaska. Rep. Invest. 5, 1–45.
Schneider, D.J., Hoblitt, R.P., 2013. Doppler weather radar observations of the 2009 eruption of Redoubt Volcano, Alaska. J. Volcanol. Geotherm. Res. 259, 133–144.
Scott, W.E., McGimsey, R.G., 1994. Character, mass, distribution, and origin of tephra-fall deposits of the 1989–1990 eruption of Redoubt Volcano, south-central Alaska. J. Volcanol. Geotherm. Res. 62, 251–272.
Sherburn, S., Bannister, S., Bibby, H., 2003. Seismic velocity structure of the central Taupo Volcanic Zone, New Zealand, from local earthquake tomography. J. Volcanol. Geotherm. Res. 122, 69–88.
Sparks, R.S.J., 2003. Forecasting volcanic eruptions. Earth Planet. Sci. Lett. 210, 1–15.
Stephens, C.D., Chouet, B.A., 2001. Evolution of the December 14, 1989 precursory long-period event swarm at Redoubt Volcano, Alaska. J. Volcanol. Geotherm. Res. 109, 133–148.
Stephens, C.D., Chouet, B.A., Page, R.A., Lahr, J.C., Power, J.A., 1994. Seismological aspects of the 1989–1990 eruptions at Redoubt Volcano, Alaska: the SSAM perspective. J. Volcanol. Geotherm. Res. 62, 153–182.
Sudo, Y., Kong, L., 2001. Three-dimensional seismic velocity structure beneath Aso Volcano, Kyushu, Japan. Bull. Volcanol. 63, 326–344.
Takei, Y., 2002. Effect of pore geometry on V_P/V_S: From equilibrium geometry to crack. J. Geophys. Res.: Solid Earth 107, 2043. https://doi.org/10.1029/2001JB000522.
Till, A.B., Yount, M.E., Bevier, M.L., 1994. The geologic history of Redoubt Volcano, Alaska. J. Volcanol. Geotherm. Res. 62, 11–30.
Unglert, K., Savage, M.K., Fournier, N., Ohkura, T., Abe, Y., 2011. Shear wave splitting, V_P/V_S, and GPS during a time of enhanced activity at Aso caldera, Kyushu. J. Geophys. Res.: Solid Earth 116, B11203. https://doi.org/10.1029/2011JB008520.
Wallace, K.L., Schaefer, J.R., Coombs, M.L., 2013. Character, mass, distribution, and origin of tephra-fall deposits from the 2009 eruption of Redoubt Volcano, Alaska-Highlighting the significance of particle aggregation. J. Volcanol. Geotherm. Res. 259, 145–169.
Werner, C., Kelly, P.J., Doukas, M., Lopez, T., Pfeffer, M., McGimsey, R., Neal, C., 2013. Degassing of CO_2, SO_2, and H_2S associated with the 2009 eruption of Redoubt Volcano, Alaska. J. Volcanol. Geotherm. Res. 259, 270–284.
Wessels, R.L., Vaughan, R.G., Patrick, M.R., Coombs, M.L., 2013. High-resolution satellite and airborne thermal infrared imaging of precursory unrest and 2009 eruption at Redoubt Volcano, Alaska. J. Volcanol. Geotherm. Res. 259, 248–269.
Wiemer, S., McNutt, S.R., 1997. Variations in the frequency-magnitude distribution with depth in two volcanic areas: Mount St. Helens, Washington, and Mt. Spurr, Alaska. Geophys. Res. Lett. 24, 189–192.
Wolf, K.J., Eichelberger, J.C., 1997. Syneruptive mixing, degassing, and crystallization at Redoubt Volcano, eruption of December, 1989 to May 1990. J. Volcanol. Geotherm. Res. 75, 19–37.
Woods, A.W., Kienle, J., 1994. The dynamics and thermodynamics of volcanic clouds: theory and observations from the April 15 and April 21, 1990 eruptions of Redoubt Volcano, Alaska. J. Volcanol. Geotherm. Res. 62, 273–299.
Young, S.R., Sparks, R.S.J., Aspinall, W.P., Lynch, L.L., Miller, A.D., Robertson, R.E., Shepherd, J.B., 1998. Overview of the eruption of Soufriere Hills volcano, Montserrat, 18 July 1995 to December 1997. Geophys. Res. Lett 25, 3389–3392.